

A Source of Indistinguishable Time-Bin Entangled Photons from a Waveguide-Embedded Quantum Dot

Martin Hayhurst Appel,¹ Alexey Tiranov,¹ Simon Pabst,¹ Ming Lai Chan,¹ Christian Starup,¹ Ying Wang,¹ Leonardo Midolo,¹ Konstantin Tiurev,¹ Sven Scholz,² Andreas D. Wieck,² Arne Ludwig,² Anders Søndberg Sørensen,¹ and Peter Lodahl¹

¹*Center for Hybrid Quantum Networks (Hy-Q), The Niels Bohr Institute, University of Copenhagen, DK-2100 Copenhagen Ø, Denmark*

²*Lehrstuhl für Angewandte Festkörperphysik, Ruhr-Universität Bochum, Universitätsstraße 150, 44801 Bochum, Germany*
(Dated: November 25, 2021)

Deterministic sources of multi-photon entanglement are highly attractive for quantum information processing but are challenging to realize experimentally. In this paper, we demonstrate a route towards a scalable source of time-bin encoded Greenberger-Horne-Zeilinger and linear cluster states from a solid-state quantum dot embedded in a nanophotonic crystal waveguide. By utilizing a self-stabilizing double-pass interferometer, we measure a spin-photon Bell state with $(67.8 \pm 0.4)\%$ fidelity and devise steps for significant further improvements. By employing strict resonant excitation, we demonstrate a photon indistinguishability of $(95.7 \pm 0.8)\%$, which is conducive to fusion of multiple cluster states for scaling up the technology and producing more general graph states.

A near-deterministic source of multi-photon entanglement will enable significant advancements in quantum information processing such as one-way quantum computing consuming few-photon Greenberger-Horne-Zeilinger (GHZ) states [1, 2] or one-way photonic repeaters relying on large photonic graph states [3, 4]. Until now, spontaneous parametric down-conversion has been the leading source of entangled photons and has enabled demonstrations of 12 entangled photons [5]. However, this approach is based on probabilistic photon sources and is thus challenging to scale up. An alternative approach proposed by Lindner and Rudolph exploits a single solid-state quantum emitter as an on-demand entanglement source [6]. In their proposal, a semiconductor quantum dot (QD) containing a single spin is repeatedly excited to create a linear cluster state of polarisation encoded photons. Despite its elegance, this approach has several experimental drawbacks. Specifically, natural spin precession is employed in a weak external magnetic field for which the QD spin is poorly decoupled from the nuclear spin bath [7–9]. Additionally, the need to collect two orthogonally polarized modes is often experimentally incompatible with the resonant excitation required for high photon indistinguishability [10]. These challenges were partly combated in the landmark experiment of Ref. [11], where the use of dark-exciton states and non-resonant excitation enabled the explicit demonstration of three-qubit entanglement and extrapolation to five qubits. Nonetheless, the further scalability of multi-photon entanglement sources has been an open question so far only addressed theoretically [12, 13]. A key feature is the generation of high-fidelity multi-photon entanglement while preserving photon indistinguishability; a crucial requirement for fusion-based photonic quantum computing [1, 14].

In this paper, we perform the first demonstration of QD spin-photon entanglement using a time-bin protocol

capable of generating multi-photon GHZ and linear cluster states. The protocol is analyzed in Refs. [12, 13] and the first experimental steps were implemented with a micropillar QD source [15] while spin-photon Bell-state generation was realized with nitrogen-vacancy centers [16, 17]. Contrary to the Lindner–Rudolph protocol, we apply strong magnetic fields which permit the use of spin-echo pulses and render the protocol insensitive to spin-dephasing [12]. Additionally, a single optical transition is excited resonantly and emits highly indistinguishable photons into a single-mode photonic crystal waveguide (PCW) with near-unity internal collection efficiency [18, 19]. Here, we focus on measuring spin-photon Bell states using a novel double-pass interferometer and determine a raw (corrected) fidelity of $65.7\%(67.8\%)$. This fidelity is predominantly limited by the quality of the spin rotations, which can be substantially improved in future experiments [20].

The entanglement protocol builds upon our recent work on uniting optical cycling transitions with optical spin control [21], as summarised in FIG. 1a. A positively charged InAs QD in an in-plane (Voigt geometry) magnetic field $B_y = 2$ T gives rise to a pair of Zeeman-split heavy-hole ground states $|\uparrow\rangle$ and $|\downarrow\rangle$, which are used as a spin qubit [22], and a pair of Zeeman-split trions $|\uparrow\uparrow\downarrow\rangle$ and $|\downarrow\uparrow\downarrow\rangle$ enabling photon generation. The four linear dipoles are driven by a red-detuned Raman laser to rotate the spin qubit [20] while the PCW (FIG. 1b) selectively enhances the optical transitions resulting in the optical cyclicity $C = \gamma_y/\gamma_x = 14.7 \pm 0.2$ [21], which is otherwise unity in a bulk environment. Spin-photon entanglement is then generated according to the protocol in FIG. 1c. Optical pumping initializes $|\downarrow\rangle$ and a $\hat{R}_y(\pi/2)$ rotation around the y-axis prepares the superposition state $(|\downarrow\rangle + |\uparrow\rangle)/\sqrt{2}$. The QD is

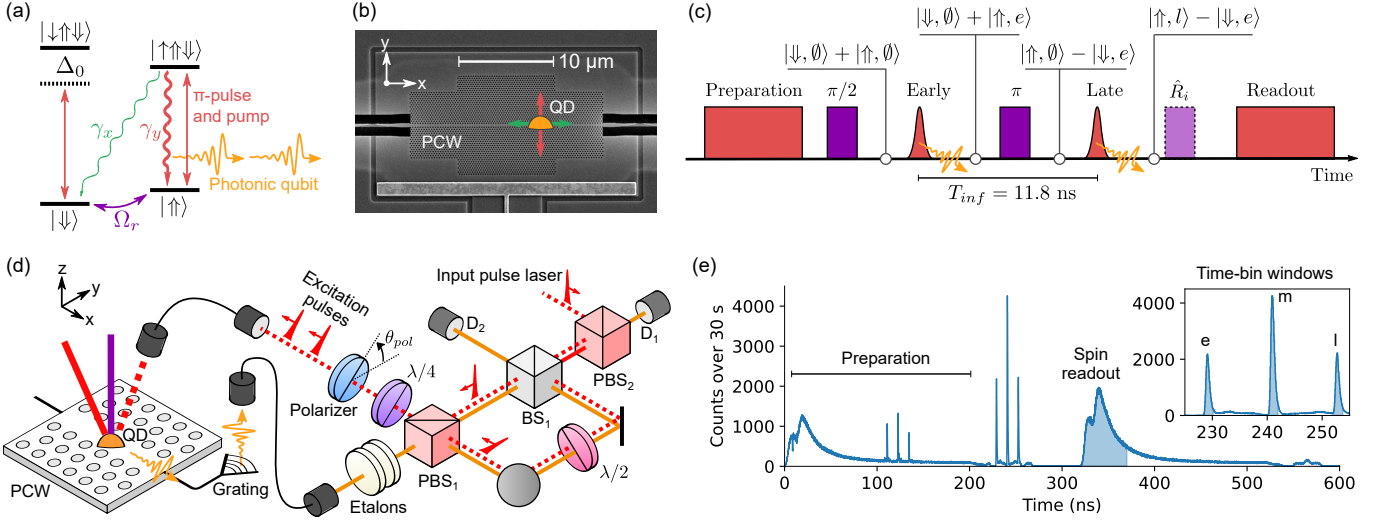


FIG. 1. (color online) Time-bin entanglement protocol. **(a)** Energy level diagram of a positively charged QD in a Voigt magnetic field. The $|\uparrow\rangle \leftrightarrow |\uparrow\uparrow\downarrow\rangle$ transition is used to emit photonic qubits and to perform spin initialisation and readout via optical pumping. The trion decay paths have rates γ_y and γ_x , Ω_r is the spin Rabi frequency and Δ_0 is the sum of the Zeeman splittings. **(b)** Scanning electron micrograph of the PCW with QD dipoles overlaid. **(c)** Experimental pulse sequence consisting of pumping pulses (red squares), rotation pulses (purple squares) and fast optical π -pulses (red pulses). The spin-photon state is indicated on top with $|\emptyset\rangle$ denoting photon vacuum and $|e\rangle$ ($|l\rangle$) denoting an early(late) photon. **(d)** Experimental setup. The PCW embedded QD is subjected to lasers propagating from free space. A double-pass TBI defines the excitation pulses (dashed red line) and interferes the emitted photons (solid orange line) resulting in mutual phase stability. A polariser with angle θ_{pol} determines the photonic readout basis. $\lambda/2(\lambda/4)$ denotes half(quarter)-waveplates. **(e)** Fluorescence histogram resulting from Bell state generation summed over both detectors including a 50 ns spin readout detection window (shaded area). The inset shows a magnified view of the early(e), middle(m) and late(l) detection windows (2 ns each) which herald the measurement basis of the photonic qubit. The peaks at 120 ns are optical reflections inside the TBI.

then subjected to a y-polarised optical π -pulse resonant with $|\uparrow\rangle \leftrightarrow |\uparrow\uparrow\downarrow\rangle$. As the other y-polarised transition is detuned by $\Delta_0 = 2\pi \times 17 \text{ GHz}$, trion excitation and thus photon emission is conditioned on $|\uparrow\rangle$. The enhanced cyclicity ensures photon emission via the spin-preserving $|\uparrow\uparrow\downarrow\rangle \rightarrow |\uparrow\rangle$ transition with probability $C/(C+1) \approx 94\%$. Thus, an early excitation entangles $|\uparrow\rangle$ with an early photon $|e\rangle$. The spin states are then swapped by a π -rotation before applying a late excitation pulse resulting in the emission of a late photon $|l\rangle$. The resulting state is the spin-photon Bell state

$$|\psi_{Bell}\rangle = (e^{i\phi_e} |\uparrow, l\rangle - |\downarrow, e\rangle)/\sqrt{2}, \quad (1)$$

where the emission time of the single photon is maximally entangled with the hole spin and ϕ_e is the phase difference between the two excitation pulses. Note that the spin does not undergo precession as we work in the rotating frame of the Raman laser. The spin thus only rotates when we actively apply a Raman pulse in contrast to Refs. [6, 11].

The entangled state is analyzed using the setup in FIG. 1d. The QD is held at 4 K in a closed cycle cryostat and emits photons into the guided PCW mode, which is coupled to a single-mode fiber via a grating coupler [23]. From here, the photon stream enters a time-bin interferometer (TBI) where a polarising beamsplitter PBS_1

gives an equal probability of transmission and reflection. This passive routing leads to three detection windows (see FIG. 1e) which herald the photonic measurement basis. An early(late) detection corresponds to an early(late) photon propagating through the short(long) interferometer arm and thus constitutes a Z-basis measurement. By contrast, the middle window represents the time-bin encoded photon interfering with itself on BS_1 . A photon click on detector D_1 or D_2 thus projects the photon onto $|\phi^\pm\rangle = (|e\rangle \pm e^{i\phi_d} |l\rangle)/\sqrt{2}$ where ϕ_d is the interferometer phase. Rather than stabilizing the TBI [16, 24] or monitoring its phase [17] we utilize a second pass through the TBI (dashed line in FIG. 1d) which derives the early and late excitation pulses from a single input pulse [25]. As a result, the phases ϕ_d and ϕ_e experience the same drift and are thus mutually stable resulting in a stable detection pattern. The long arm delay $T_{inf} = 11.8 \text{ ns}$ defines the time-bin separation and is sufficient for performing photon emission (400 ps lifetime) and π -rotations (7 ns) between the early and late excitations. The TBI also includes two 3 GHz FWHM etalon filters which reject the Raman laser scatter and the QD phonon sideband [26].

We now proceed to quantify the spin-photon entanglement using the approach of Ref. [27] in which the fidelity of an N -qubit GHZ state may be exactly determined with only $N+1$ measurement settings. Adapting

the technique to a Bell state gives

$$\mathcal{F}_{Bell} = \frac{\langle \hat{P}_z \rangle}{2} + \frac{\langle \hat{M}_y \rangle - \langle \hat{M}_x \rangle}{4}, \quad (2)$$

using the operators $\hat{P}_z = |\uparrow\rangle\langle\uparrow| + |\downarrow\rangle\langle\downarrow|$, $\hat{M}_x = \hat{\sigma}_x^{(s)} \otimes \hat{\sigma}_x^{(p)}$ and $\hat{M}_y = \hat{\sigma}_y^{(s)} \otimes \hat{\sigma}_y^{(p)}$, where $\hat{\sigma}$ denotes single qubit pauli matrices, s(p) superscripts denote spin(photonic) qubit, and we designate the logical qubits $|0\rangle = |\uparrow\rangle, |l\rangle$ and $|1\rangle = |\downarrow\rangle, |e\rangle$. We post-select on measuring photons in both the photonic and spin readout windows and achieve a 124 Hz coincidence rate when repeating the experiment at a 1.65 MHz repetition rate. As the spin readout can only detect $|\uparrow\rangle$ we apply a \hat{R}_i rotation prior to readout (FIG. 1c) fulfilling $\hat{R}_i|s\rangle = |\uparrow\rangle$ to realize the desired spin projector $|s\rangle\langle s|$. FIG. 2a shows the results of a ZZ-basis measurement. Projection on $|e\rangle$ and $|l\rangle$ is given by the photon detection time (both detectors are treated equally) and the \hat{R}_i pulse is toggled between a 0 and a π rotation to realize projections onto $|\uparrow\rangle$ and $|\downarrow\rangle$, respectively. Normalizing across all four projections yields $\langle \hat{P}_z \rangle = (89.3 \pm 0.4)\%$. The imbalance of $|\uparrow\rangle|l\rangle$ and $|\downarrow\rangle|e\rangle$ is primarily a consequence of the imperfect \hat{R}_i spin rotation (discussed later) which reduces the probability of measuring $|\downarrow\rangle$.

In order to measure time-bin encoded photons in the equatorial plane of the Bloch sphere, we add a controllable phase difference between the early and late excitation pulses. These pulses are orthogonally polarized upon encountering PBS₁ (FIG. 1d) but are projected onto the transmission axis of a rotatable polarizer, which adds $2\theta_{pol}$ to the phase ϕ_e . FIG. 2b shows the TBI detection pattern when the classical excitation pulses are reinjected into the detection pass and reveals a near-perfect visibility. The angle $\theta_{pol} = \theta_0$ corresponds to the condition $\phi_d = \phi_e$ and depends on the precise TBI alignment but is stable on a week timescale. We then run the entanglement protocol, project the QD spin onto $|\pm X\rangle_s = (|\uparrow\rangle \pm |\downarrow\rangle)/\sqrt{2}$ (for $\hat{R}_i = \hat{R}_y(\pm\pi/2)$) and measure the spin state dependent contrast, see FIG. 2b. Crucially, the two fringes are perfectly in-phase and out-of-phase with the classical TBI response. In summary, measuring the photon in the X-basis corresponds to setting $\theta_{pol} = \theta_0$ and assigning the photon states $|+X\rangle_p$ and $|-X\rangle_p$ to a middle window detection on D₁ and D₂, respectively. FIG. 2c shows the outcomes of an XX-basis measurement. The outcomes are normalized as before and the probability difference between the positive and negative eigenstates of \hat{M}_x results in $\langle \hat{M}_x \rangle = (-42.3 \pm 1.1)\%$. The \hat{M}_y measurement is similarly realized by setting $\theta_{pol} = \theta_0 + \pi/4$ and $\hat{R}_i = \hat{R}_x(\pm\pi/2)$ leading to $\langle \hat{M}_y \rangle = (42.1 \pm 1.1)\%$. By applying Eq. (2) we arrive at the final estimate $\mathcal{F}_{Bell}^{raw} = (65.7 \pm 0.4)\%$ which exceeds the classical threshold of 50% by 39 standard deviations using only 6 minutes of acquisition and no corrections. We note that

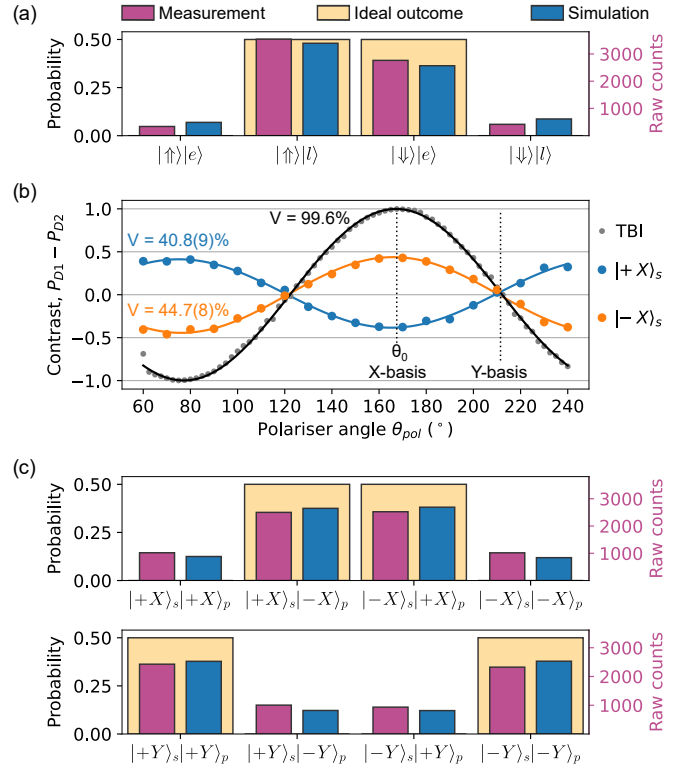


FIG. 2. (color online) Entanglement verification. **(a)** Spin-photon Bell state measured in ZZ-basis. Magenta bars denote the measured spin-photon coincidences during a 120 s acquisition. The right y-axis indicates raw counts and the left y-axis shows the probability normalized across all four outcomes. The yellow and blue bars represent the ideal and simulated detection patterns, respectively. **(b)** Determination of the photonic readout basis. The y-axis indicates the normalized intensity difference between the two TBI detectors in the middle window. The gray dots show the TBI response to a classical input while the blue and orange curves denote spin-photon coincidences when projecting the spin on $|\pm X\rangle_s$ (legend). The fits follow $V \cos(2(\theta_{pol} - \theta_0))$. Errorbars are within the datapoints. **(c)** Spin-photon measurements in the XX-basis (top row) and YY-basis (bottom row). The s and p subscripts denote spin and photonic qubit, respectively. Axes and legends follow (a).

some of the recorded spin-photon coincidences are due to uncorrelated laser leakage. However, this contribution is minor and correcting for the background (as in Ref. [17]) leads to a corrected fidelity of $\mathcal{F}_{Bell}^{corr} = (67.8 \pm 0.4)\%$. NV centers [16, 17] have produced similar quality Bell states but with greater reliance on background subtraction. To test our understanding of the error mechanisms we perform a Monte Carlo simulation of the experiment including all errors and backgrounds (detailed in Supplemental materials). This yields the fidelity $\mathcal{F}_{Bell}^{sim} = 67.8\%$ (comparable with \mathcal{F}_{Bell}^{raw}) and the detection pattern in FIG. 2 which is in good agreement with the experimental values and supports our error analysis.

We now highlight two of the errors limiting \mathcal{F}_{Bell} . Our dominant error is the quality of our Raman pulses which is characterized in the Supplemental materials and Ref. [21]. By measuring the dampening of Rabi oscillations between $|\uparrow\rangle$ and $|\downarrow\rangle$ we extract a π -pulse fidelity of $F_\pi = 88.5\%$ which is predominantly limited by incoherent spin-flips between the two spin states. Naturally, the time-bin protocol relies on highly coherent spin control, and $F_\pi = 88.5\%$ alone limits the Bell state fidelity to 77% according to Monte Carlo simulations. Thus, we may attribute $\sim 70\%$ of the measured infidelity to this mechanism. Fortunately, a recent scheme using electron spins and nuclear spin cooling [20] demonstrated $F_\pi = 98.8\%$ and could readily be implemented in the experimental protocol. This would increase the achievable fidelity to $\mathcal{F}_{Bell} = 97.3\%$ (neglecting other errors).

A second relevant error is the single-photon purity and indistinguishability of the emitted photons. This error is particularly relevant for combining multiple smaller cluster states through entanglement fusion [2]. To accurately characterize the time-bin encoded photon, we retain the magnetic field and minimally modify the pulse sequence to emit two separable single photons (FIG. 3a). By using the TBI, we simultaneously measure the $g^{(2)}$ intensity autocorrelation and Hong-Ou-Mandel (HOM) visibility by letting the detection time herald the experiment. FIG. 3b shows the delays between photons recorded in either the early or late detection windows and constitutes two sets of $g^{(2)}$ measurements. A slight bunching is observed for short delays owing to non-deterministic initialization of the hole charge state and the minor proclivity for coincidences in the early data set is a consequence of the finite cyclicity. Normalizing $g^{(2)}$ at long delays and averaging over early and late gives $g^{(2)}(0) = (4.7 \pm 0.6)\%$ from which 1.1% may be attributed to excitation laser scatter. The remaining contribution is likely a result of multi-photon emission owing to the fast, Purcell enhanced decay rate $\gamma_0 = (\gamma_x + \gamma_y) = 2.54 \text{ ns}^{-1}$ and the FWHM duration of the π -pulse $T_{opt} = 35 \text{ ps}$. T_{opt} represents a trade-off [12, 13] between multi-photon emission (minimized for $T_{opt} \ll \gamma_0^{-1}$) and unwanted excitation of $|\downarrow\rangle \leftrightarrow |\downarrow\uparrow\downarrow\rangle$ (minimized for $T_{opt} \gg \Delta_0^{-1}$). A larger magnetic field will increase Δ_0 and permit a shorter T_{opt} and thus reduced $g^{(2)}(0)$. FIG. 3c shows the delay between two photons recorded within the same experimental repetition when at least one photon was measured in the middle window. Following Ref. [28], this estimates a raw indistinguishability of $\mathcal{V}^{raw} = 1 - 2N_2/(N_1 + N_3) = (86.5 \pm 0.6)\%$ (integration windows given in FIG. 3c). \mathcal{V}^{raw} is primarily limited by the finite $g^{(2)}(0)$ according to $\mathcal{V}^{raw} \approx \mathcal{V}/(1 + 2g^{(2)}(0))$, which assumes the multi-photon contribution to consist of distinguishable photons [28, 29]. Correcting

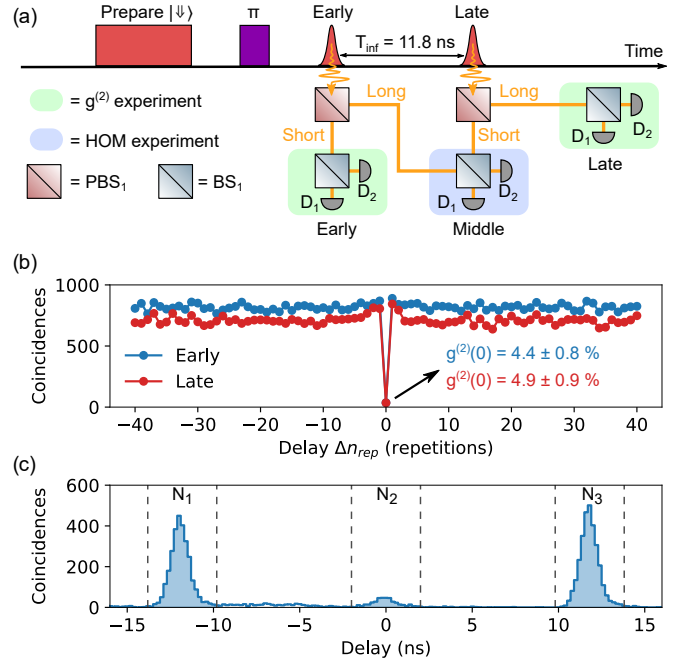


FIG. 3. (color online) Single-photon characterisation. (a) Pulse sequence for $g^{(2)}$ and HOM measurements. A pump and a Raman pulse prepares $|\uparrow\rangle$ and optical π -pulses are used to emit two photons. The TBI (here in a path-representation) can either measure a single photon on a BS ($g^{(2)}$ measurement) or interfere two photons on a BS (HOM measurement). Waveplates (not shown) ensure identical polarization at the middle detection. (b) $g^{(2)}$ measurement results. The x-axis indicates the delay between photons in units of the experimental repetition time. (c) Photon coincidences within the same experimental repetition yielding a HOM measurement.

for $g^{(2)}(0)$ and the slight imperfection of the TBI yields a corrected HOM visibility of $\mathcal{V} = (95.7 \pm 0.8)\%$ which is compatible with the QD state of the art [30–32].

In summary, we have used a PCW embedded QD to implement a scalable protocol for the generation of time-bin entangled photonic states. This is facilitated by the PCW platform which offers a compelling marriage of spin control and photonic enhancement. Operating at high magnetic fields allows spin initialization without projective measurements and the photon indistinguishability is independent of the magnetic field strength as a single optical transition is used for emission. Our insights from theory and simulation show a clear path towards improving the fidelity with the quality of spin rotations requiring the most attention. Indeed, given realistic PCW parameters and greatly enhanced Raman pulses we expect to reach an error level of 2.1% per emitted photon [13]. The generalization to more photons is straightforward and only requires additional rotation and excitation pulses to create a multi-photon GHZ or 1D-cluster state with photonic qubits emitted

every 28 ns. We have attempted a three-qubit GHZ state (Supplemental materials) but only measured a $\mathcal{F}_{GHZ} = (42.3 \pm 1.4)\%$ fidelity due to the imperfect Raman pulses.

Another promising aspect of our approach is the entanglement generation rate. Our 124 Hz Bell-state detection rate is already favourable against similar protocols based on NV centers (7 mHz in Ref. [17]) despite our limited and non-optimized total detection efficiency $\eta_{total} = 0.3\%$. Indeed, a QD-to-fiber collection efficiency of $\eta = 7\%$ was recently demonstrated in a similar PCW structure and further realistic improvements may facilitate collection efficiencies as high as $\eta = 78\%$ [32]. Finally, we note that the high magnetic field regime can give access to nuclear magnon modes [33], which may be used as a long-lived quantum memory for repeater applications or as an ancillary qubit for use in photonic graph state generation [34, 35].

The data presented in this manuscript are available at [?].

The authors thank Alisa Javadi, Matthias C. Löbl and Richard J. Warburton for valuable discussions. We gratefully acknowledge financial support from Danmarks Grundforskningsfond (DNRF 139, Hy-Q Center for Hybrid Quantum Networks), Styrelsen for Forskning og Innovation (FI) (5072-00016B QUANTECH), the European Union's Horizon 2020 research and innovation programme under grant agreement No. 820445 and project name Quantum Internet Alliance, the European Union's Horizon 2020 Research and Innovation programme under grant agreement No. 861097 (project name QUDOT-TECH). SS, ADW and AL gratefully acknowledge financial support from Deutsche Forschungsgemeinschaft (DFG) (TRR 160 and LU2051/1-1) and the grants QR.X KIS6QK4001 and DFH/UFA CDFA-05-06.

-
- [1] M. Gimeno-Segovia, P. Shadbolt, D. E. Browne, and T. Rudolph, From Three-Photon Greenberger-Horne-Zeilinger States to Ballistic Universal Quantum Computation, *Phys. Rev. Lett.* **115**, 020502 (2015).
 - [2] T. Rudolph, Why i am optimistic about the silicon-photonics route to quantum computing, *APL Photonics* **2**, 030901 (2017).
 - [3] J. Borregaard, H. Pichler, T. Schröder, M. D. Lukin, P. Lodahl, and A. S. Sørensen, One-way quantum repeater based on near-deterministic photon-emitter interfaces, *Phys. Rev. X* **10**, 021071 (2020).
 - [4] K. Azuma, K. Tamaki, and H.-K. Lo, All-photonics quantum repeaters, *Nat. Commun.* **6**, 6787 (2015).
 - [5] H. S. Zhong, Y. Li, W. Li, L. C. Peng, Z. E. Su, Y. Hu, Y. M. He, X. Ding, W. Zhang, H. Li, L. Zhang, Z. Wang, L. You, X. L. Wang, X. Jiang, L. Li, Y. A. Chen, N. L. Liu, C. Y. Lu, and J. W. Pan, 12-Photon Entanglement and Scalable Scattershot Boson Sampling with Optimal Entangled-Photon Pairs from Parametric Down-Conversion, *Phys. Rev. Lett.* **121**, 250505 (2018).
 - [6] N. H. Lindner and T. Rudolph, Proposal for pulsed On-demand sources of photonic cluster state strings, *Phys. Rev. Lett.* **103**, 113602 (2009).
 - [7] R. Stockill, C. Le Gall, C. Matthiesen, L. Huthmacher, E. Clarke, M. Hugues, and M. Atatüre, Quantum dot spin coherence governed by a strained nuclear environment, *Nat. Commun.* **7**, 1 (2016).
 - [8] J. H. Prechtel, A. V. Kuhlmann, J. Houel, A. Ludwig, S. R. Valentin, A. D. Wieck, and R. J. Warburton, Decoupling a hole spin qubit from the nuclear spins, *Nat. Mater.* **15**, 981 (2016).
 - [9] L. Huthmacher, R. Stockill, E. Clarke, M. Hugues, C. LeGall, and M. Atatüre, Coherence of a dynamically decoupled quantum-dot hole spin, *Phys. Rev. B* **97**, 241413(R) (2018).
 - [10] Y. M. He, Y. J. Wei, D. Wu, M. Atatüre, C. Schneider, S. Höfling, M. Kamp, C. Y. Lu, and J. W. Pan, On-demand semiconductor single-photon source with near-unity indistinguishability, *Nat. Nanotechnol.* **8**, 213 (2013).
 - [11] I. Schwartz, D. Cogan, E. R. Schmidgall, Y. Don, L. Gantz, O. Kenneth, N. H. Lindner, and D. Gershoni, Deterministic generation of a cluster state of entangled photons., *Science* (80-.). **354**, 434 (2016).
 - [12] K. Tiurev, P. L. Mirambell, M. B. Lauritzen, M. H. Appel, A. Tiranov, P. Lodahl, and A. S. Sørensen, Fidelity of time-bin entangled multi-photon states from a quantum emitter, *Phys. Rev. A* **104**, 052604 (2021).
 - [13] K. Tiurev, M. H. Appel, P. L. Mirambell, M. B. Lauritzen, A. Tiranov, P. Lodahl, and A. S. Sørensen, High-fidelity multi-photon-entangled cluster state with solid-state quantum emitters in photonic nanostructures, (2021), [arXiv:2007.09295](https://arxiv.org/abs/2007.09295).
 - [14] R. Uppu, L. Midolo, X. Zhou, J. Carolan, and P. Lodahl, Quantum-dot-based deterministic photon-emitter interfaces for scalable photonic quantum technology, *Nat. Nanotechnol.* **10.1038/s41565-021-00965-6** (2021).
 - [15] J. P. Lee, B. Villa, A. J. Bennett, R. M. Stevenson, D. J. P. Ellis, I. Farrer, D. A. Ritchie, and A. J. Shields, A quantum dot as a source of time-bin entangled A quantum dot as a source of time-bin entangled multi-photon states, *Quantum Sci. Technol* **4**, 025011 (2019).
 - [16] A. Tchebotareva, S. L. Hermans, P. C. Humphreys, D. Voigt, P. J. Harmsma, L. K. Cheng, A. L. Verlaan, N. Dijkhuizen, W. De Jong, A. Dréau, and R. Hanson, Entanglement between a Diamond Spin Qubit and a Photonic Time-Bin Qubit at Telecom Wavelength, *Phys. Rev. Lett.* **123**, 063601 (2019).
 - [17] R. Vasconcelos, S. Reisenbauer, C. Salter, G. Wachter, D. Wirtitsch, J. Schmiedmayer, P. Walther, and M. Trupke, Scalable spin-photon entanglement by time-to-polarization conversion, *npj Quantum Inf.* **6**, 9 (2020).
 - [18] M. Arcari, I. Söllner, A. Javadi, S. Lindskov Hansen, S. Mahmoodian, J. Liu, H. Thyrrstrup, E. H. Lee, J. D. Song, S. Stobbe, and P. Lodahl, Near-Unity Coupling Efficiency of a Quantum Emitter to a Photonic Crystal Waveguide, *Phys. Rev. Lett.* **113**, 093603 (2014).
 - [19] P. Lodahl, S. Mahmoodian, and S. Stobbe, Interfacing single photons and single quantum dots with photonic nanostructures, *Rev. Mod. Phys.* **87**, 347 (2015).
 - [20] J. H. Bodey, R. Stockill, E. V. Denning, D. A. Gangloff, G. Éthier-Majcher, D. M. Jackson, E. Clarke, M. Hugues,

- C. L. Gall, and M. Atatüre, Optical spin locking of a solid-state qubit, *npj Quantum Inf.* **5**, 95 (2019).
- [21] M. H. Appel, A. Tiranov, A. Javadi, M. C. Löbl, Y. Wang, S. Scholz, A. D. Wieck, A. Ludwig, R. J. Warburton, and P. Lodahl, Coherent Spin-Photon Interface with Waveguide Induced Cycling Transitions, *Phys. Rev. Lett.* **126**, 013602 (2021).
- [22] R. J. Warburton, Single spins in self-assembled quantum dots, *Nat. Mater.* **12**, 483 (2013).
- [23] X. Zhou, I. Kulkova, T. Lund-Hansen, S. L. Hansen, P. Lodahl, and L. Midolo, High-efficiency shallow-etched grating on GaAs membranes for quantum photonic applications, *Appl. Phys. Lett.* **113**, 251103 (2018).
- [24] F. Vedovato, C. Agnesi, M. Tomasin, M. Avesani, J. Å. Larsson, G. Vallone, and P. Villoresi, Postselection-Loophole-Free Bell Violation with Genuine Time-Bin Entanglement, *Phys. Rev. Lett.* **121**, 190401 (2018).
- [25] H. Jayakumar, A. Predojević, T. Kauten, T. Huber, G. S. Solomon, and G. Weihs, Time-bin entangled photons from a quantum dot, *Nat. Commun.* **5**, 4251 (2014).
- [26] G. Kiršanskė, H. Thyrrestrup, R. S. Daveau, C. L. Dreeßen, T. Pregolato, L. Midolo, P. Tighineanu, A. Javadi, S. Stobbe, R. Schott, A. Ludwig, A. D. Wieck, S. I. Park, J. D. Song, A. V. Kuhlmann, I. Söllner, M. C. Löbl, R. J. Warburton, and P. Lodahl, Indistinguishable and efficient single photons from a quantum dot in a planar nanobeam waveguide, *Phys. Rev. B* **96**, 165306 (2017).
- [27] O. Gühne, C. Y. Lu, W. B. Gao, and J. W. Pan, Toolbox for entanglement detection and fidelity estimation, *Phys. Rev. A* **76**, 030305(R) (2007).
- [28] C. Santori, D. Fattal, J. Vučković, G. S. Solomon, and Y. Yamamoto, Indistinguishable photons from a single-photon device, *Nature* **419**, 594 (2002).
- [29] H. Ollivier, S. E. Thomas, S. C. Wein, I. Maillette de Buy Wenniger, N. Coste, J. C. Lored, N. Somaschi, A. Harouri, A. Lemaitre, I. Sagnes, L. Lanco, C. Simon, C. Anton, O. Krebs, and P. Senellart, Hong-Ou-Mandel Interference with Imperfect Single Photon Sources, *Phys. Rev. Lett.* **126**, 063602 (2021).
- [30] X. Ding, Y. He, Z. C. Duan, N. Gregersen, M. C. Chen, S. Unsleber, S. Maier, C. Schneider, M. Kamp, S. Höfling, C. Y. Lu, and J. W. Pan, On-Demand Single Photons with High Extraction Efficiency and Near-Unity Indistinguishability from a Resonantly Driven Quantum Dot in a Micropillar, *Phys. Rev. Lett.* **116**, 020401 (2016).
- [31] N. Tömm, A. Javadi, N. O. Antoniadis, D. Najer, M. C. Löbl, A. R. Korsch, R. Schott, S. R. Valentin, A. D. Wieck, A. Ludwig, and R. J. Warburton, A bright and fast source of coherent single photons, *Nat. Nanotechnol.* **16**, 399 (2021).
- [32] R. Uppu, F. T. Pedersen, Y. Wang, C. T. Olesen, C. Papon, X. Zhou, L. Midolo, S. Scholz, A. D. Wieck, A. Ludwig, and P. Lodahl, Scalable integrated single-photon source, *Sci. Adv.* **6**, eabc8268 (2020).
- [33] D. M. Jackson, D. A. Gangloff, J. H. Bodey, L. Zaporski, C. Bachorz, E. Clarke, M. Hugues, C. Le Gall, and M. Atatüre, Quantum sensing of a coherent single spin excitation in a nuclear ensemble, *Nat. Phys.* **17**, 585 (2021).
- [34] D. Buterakos, E. Barnes, and S. E. Economou, Deterministic generation of all-photonic quantum repeaters from solid-state emitters, *Phys. Rev. X* **7**, 041023 (2017).
- [35] A. Russo, E. Barnes, and S. E. Economou, Generation of arbitrary all-photonic graph states from quantum emitters, *New J. Phys.* **21**, 055002 (2019).